

Non-smooth gravity problem with total variation penalization functional

H. Bertete-Aguirre,¹ E. Cherkaev² and M. Oristaglio³

¹Livermore National Lab, PO Box 808, L-206, Livermore, CA 94551

²University of Utah, Department of Mathematics, 155 South 1400 East, JWB 233, Salt Lake City, UT84112. E-mail: elena@math.utah.edu

³Schlumberger-Doll Research, Old Quarry Road, Ridgefield, Connecticut 06877

Accepted 2001 December 7. Received 2001 November 22; in original form 1999 December 23

SUMMARY

This work deals with reconstruction of non-smooth solutions of the inverse gravimetric problem. This inverse problem is very ill-posed, its solution is non-unique and unstable. The stable inversion method requires regularization. Regularization methods commonly used in geophysics reconstruct smooth solutions even though geological structures often have sharp contrasts (discontinuities) in properties. This is the result of using a quadratic penalization term as a stabilizing functional. We introduce the total variation of the reconstructed model as a stabilizing functional that does not penalize sharp features of the solution. This approach permits reconstruction of (non-smooth) density functions that represent blocky geological structures. An adaptive gradient scheme is shown to be effective in solving the regularized inverse problem. Numerically simulated examples consisting of models with several homogeneous blocks illustrate the behaviour of the method.

Key words: gravity, inverse problem, optimization, regularization, total variation.

1 INTRODUCTION

The gravimetric inverse problem is to determine Earth's density distribution from measurements of gravity (or its derivatives) on the surface or in boreholes. This problem is (intrinsically) non-unique, and its numerical solution is unstable: small variations in the data can cause large variations in the solution. Moreover, gravity data can only be measured at discrete points and are contaminated with noise; hence there are always some deviations of the measured data from the true gravity field. Different regularization techniques have been developed to stabilize the inverse problem and ensure that the solution constructed numerically is close, in some sense, to the true solution. There is extensive literature on this subject (e.g. Tikhonov & Arsenin 1977; Lavrentiev *et al.* 1980). Inversion methods commonly used in geophysics aim to recover a smooth model by including a regularizing term that penalizes sharp changes in properties (e.g. 'Occam's' inversion; Constable *et al.* 1987). Smoothing regularization operators are based on using L_2 norms, in which case the optimization problem is quadratic; its solution is given by a solution of a linear equation. Most methods give good results for smooth models; however, they are not able to recover blocky structures or non-smooth density distributions. But blocky structures, such as faults, mineral bodies, dikes, etc., with abrupt changes of properties are often the targets of geophysical exploration. Efforts to recover sharp density contrasts in the gravimetric problem are successful when the shape of the anomalous body, its mass centre, or some other geometric characteristics are available as *a priori* information. Using such information, Green (1975) constructs a varying

background model. Last & Kubik (1983) minimize the total volume of the body of anomalous density. Guillen & Menichetti (1984) minimize the inertia of the body. In order to increase the depth resolution, depth weighting is introduced in Li & Oldenburg (1998). Portniaguine & Zhdanov (1999) discuss several other stabilization functionals.

We introduce an alternative regularization that can handle blocky geological structures with discontinuities in properties. We propose to use the total variation (TV) stabilizing functional to drive the solution to blocky structures. Use of total variation functionals was developed in image reconstruction to restore sharp edges and high contrast images (Rudin *et al.* 1992); it is also used in electrical tomography (Dobson & Santosa 1994). The variation of a function (Giusti 1984) is a total change of the values of the function in the domain. It sums up the jumps of the function at discontinuity points and its variation in the domains where the function is continuous. When the function is differentiable, its variation can be expressed as L_1 norm of the derivative in 1-D case, or of the gradient in 2- or 3-D case. Introducing a total variation functional leads to a non-quadratic minimization problem, the solution of which is more computationally expensive than the solution of a quadratic problem. We use an adaptive gradient algorithm to minimize the objective functional that combines the data misfit with the total variation of the solution. Numerical simulations show that an inversion scheme regularized by the total variation functional can reconstruct non-smooth features of the density distribution. This can be a very desirable feature for many inverse problems in geophysical exploration.

2 THE INVERSE GRAVIMETRIC PROBLEM

The inverse gravimetric problem is to determine the distribution of the density inside the earth from the measurements of the gravity field on the surface. First, consider the forward problem. Let a domain $\Omega \in R^3$ be a subsurface domain with a spatially varying density of the medium $\rho(\mathbf{r})$, $\mathbf{r} = (x, y, z)$. The gravitational potential $u(\mathbf{r})$ generated by this density function satisfies Poisson's equation inside the domain Ω :

$$\Delta u(\mathbf{r}) = -4\pi\gamma\rho(\mathbf{r}), \quad \mathbf{r} \in \Omega. \quad (1)$$

Here γ is universal gravitational constant. Further we drop constant γ as scaling does not affect the properties of solution. The coefficient 4π in the righthand side is changed to 2π when we deal with 2-D problem. Using the fundamental solution $G(\mathbf{r}', \mathbf{r})$, the solution of eq. (1) at the point \mathbf{r}' can be written as

$$u(\mathbf{r}') = \int_{\Omega} \rho(\mathbf{r})G(\mathbf{r}', \mathbf{r}) d\mathbf{r}. \quad (2)$$

Most gravimeters measure the intensity F of the gravity field (force), i.e. the component of the field in the direction of the field itself. This can be described (Backus 1968) by a non-linear boundary condition $|\nabla u| = F$. The problem is then linearized near the first approximation of the solution that is given by the gravitating mass in the centre of the Earth. Hence the linearized problem amounts to a problem with the vertical derivative of the potential u on the boundary. This corresponds well to an assumption that the measured data are values of the vertical derivative of the gravitational potential due to an anomalous mass distribution. We notice that this problem is well posed contrary to a similar problem for magnetic potential (Backus 1970), where the linearized problem is one with an oblique derivative boundary condition (Cherkaeva 1990) and the presence of magnetic equator completely changes the character of the problem.

Hence, we assume that the measured component of the gravity field, a function g , is the vertical derivative of the gravitational potential, which is related to the density ρ (see eq. 2) through the integral equation:

$$g(\mathbf{r}') = \int_{\Omega} \rho(\mathbf{r})\mathcal{K}(\mathbf{r}', \mathbf{r}) d\mathbf{r}, \quad (3)$$

where the kernel of the integral operator $\mathcal{K}(\mathbf{r}', \mathbf{r})$ in 2-D is given by:

$$\mathcal{K}(\mathbf{r}', \mathbf{r}) = \frac{\partial}{\partial z'} \ln \frac{1}{|\mathbf{r} - \mathbf{r}'|} = \frac{z - z'}{|\mathbf{r} - \mathbf{r}'|^2}, \quad (4)$$

and in 3-D case is:

$$\mathcal{K}(\mathbf{r}', \mathbf{r}) = \frac{\partial}{\partial z'} \frac{1}{|\mathbf{r} - \mathbf{r}'|} = \frac{z - z'}{|\mathbf{r} - \mathbf{r}'|^3}. \quad (5)$$

To solve the inverse problem, we need to solve the integral equation (3) with the known function g (or samples of g). Solution of this inverse problem is very non-unique. This can be easily demonstrated by representing the gravitational potential by a single layer potential imitating a thin layer of masses on the boundary of the domain Ω . In case of only Newtonian potentials (that correspond to volume mass distribution), the inverse problem is also very non-unique. We show an example demonstrating non-uniqueness of solution of this problem in Appendix A. Uniqueness can be achieved if we constrain the set of functions that can serve as density distributions. This corresponds to introducing *a priori* physical information. The first results on uniqueness of reconstruction of a starlike object of constant density are obtained by Novikov (1938). Strakhov & Brodsky

(1986) derived conditions for a unique solution of the inverse potential problem for polygonal structures. Constraints for the solution stemming from the requirement of positivity of the density function are considered by Sabatier (1977). The inverse gravity problem is a particular case of the inverse source problem, the non-uniqueness of its solution being discussed in detail by Isakov (1990).

Further we assume that we deal with the gravitational potential described by the eq. (2) and vertical component of the gravity field given by (3). Eq. (3) is a Fredholm integral equation of the first kind (for ρ) and can be written in operator form

$$K\rho = g. \quad (6)$$

The operator K is compact. Hence it can be shown that the inverse operator K^{-1} is not continuous. This implies that the solution ρ does not depend continuously on the measured data. The inverse problem is unstable as well as non-unique. We assume that non-uniqueness can be overcome in the standard way by constraining the solution space. We concentrate here on the problem of stable reconstruction of a non-smooth solution.

3 QUADRATIC STABILIZATION

A common way to solve inverse problems is by minimization of the objective functional that combines least square data misfit functional and a stabilization term penalizing non-smooth and fast oscillating solutions. To formulate an objective functional, we consider least square minimization of the data misfit

$$\min_{\rho} P(\rho, g) = \min_{\rho} \|K\rho - g\|_2^2. \quad (7)$$

To obtain a stable solution using the Tikhonov regularization approach, the penalization functional $J(\rho)$ is introduced in the problem (7). This leads to a regularized minimization problem:

$$\min_{\rho} P^{\alpha}(\rho, g) = \min_{\rho} (\|K\rho - g\|_2^2 + \alpha J(\rho)), \quad (8)$$

where α is a parameter of regularization, which depends on the data noise level and can be controlled by the interpreter. In absence of exact knowledge of the noise level, L-curve or heuristic (or empiric) methods are used (Hansen & O'Leary 1993).

The choice of the functional $J(\rho)$ is very important because it significantly influences the solution. It determines a class of functions that can be minimizers of this problem. Some popular quadratic stabilization functionals (e.g. Tikhonov & Arsenin 1977; Constable *et al.* 1987; Kolesova & Cherkaeva 1987; Bassrei 1993; Bertete-Aguirre & Xavier 1994) are the L_2 norm of the solution

$$J_0(\rho) = \|\rho\|_2^2 = \int_{\Omega} \rho^2(\mathbf{r}) d\mathbf{r}, \quad (9)$$

or the L_2 norm of its derivatives:

$$J_1(\rho) = \|\nabla\rho\|_2^2 = \int_{\Omega} |\nabla\rho(\mathbf{r})|^2 d\mathbf{r}. \quad (10)$$

Here the vector $\nabla\rho(\mathbf{r})$ is the vector of the gradient of the function $\rho(\mathbf{r})$

$$|\nabla\rho(\mathbf{r})|^2 = \rho_x^2 + \rho_y^2 + \rho_z^2. \quad (11)$$

The solution of the optimization problem (8) is provided by the solution of the Euler-Lagrange equation that can be obtained varying the functional $P^{\alpha}(\rho, g)$. As an example, we consider the problem with $J_1(\rho)$ stabilization functional. The Euler-Lagrange equation for

this problem is derived in Appendix B. It can be written in operator form convenient for discretization:

$$(K^*K - \alpha\Delta)\rho = K^*g. \quad (12)$$

Problem (12) is linear. After discretization, it can be solved by direct calculation of the inverse (or pseudo-inverse) of the matrix $(K^*K - \alpha\Delta)$. Analogous derivation for the problem with the functional J_0 leads to an equation similar to eq. (12), where identity operator takes place of the laplacian.

4 SMOOTHING BY A QUADRATIC STABILIZING FUNCTIONAL

The considered functionals effectively stabilize an otherwise unstable solution, but they perform stabilization by suppressing the high frequency content of the reconstructed function. This leads to smoothing of the recovered density function. To show this smoothing property of quadratic stabilizing functionals, we consider eq. (3) in Fourier domain. Properties of potential fields in the frequency domain are well studied in Bhattacharyya (1967), Parker (1973) and Strakhov & Valyashko (1984) among others. We assume a 3-D problem with a cartesian coordinate system, measurements are taken on the plane $S = \{(s', z') : z' = 0\}$, with $s' = (x', y')$. We take Fourier transform of both sides of (3) with the kernel \mathcal{K} given by (5):

$$\hat{g}(\mathbf{t}) = \int_{\Omega} \rho(\mathbf{r})z \int_S \frac{e^{-i(\mathbf{t}\cdot\mathbf{s}')}}{|\mathbf{s}' - \mathbf{r}|^3} d\mathbf{s}' d\mathbf{r}. \quad (13)$$

Here $(\mathbf{t} \cdot \mathbf{s}') = \tau_1 x' + \tau_2 y'$ with $\mathbf{t} = (\tau_1, \tau_2)$ being Fourier frequencies. From Erdelyi *et al.* (1954), the integral over S can be estimated, yielding:

$$\hat{g}(\mathbf{t}) = 2\pi \int_{\Omega} \rho(s', z) e^{-i(\mathbf{t}\cdot\mathbf{s}')} e^{-\tau z} ds' dz, \quad \tau = |\mathbf{t}|. \quad (14)$$

To continue, we simplify the model and assume that the density ρ is confined to a volume between two horizontal planes at the levels z_1 and z_2 , $z_1 < z_2$, and in this volume, is constant in vertical direction, $\rho(x, y, z) = \rho(x, y)$ for $z \in (z_1, z_2)$. Then,

$$\hat{g}(\mathbf{t}) = 2\pi \int_S \int_{z_1}^{z_2} \rho(s', z) e^{-i(\mathbf{t}\cdot\mathbf{s}')} e^{-\tau z} ds' dz. \quad (15)$$

For this model, calculation of the last integral immediately gives,

$$\hat{g}(\mathbf{t}) = \hat{\rho}(\mathbf{t}) e^{-\tau z_1} \eta \tau^{-1}, \quad \eta = (1 - e^{-\tau \Delta z}), \quad (16)$$

with $\Delta z = z_2 - z_1$. The reconstruction of the function ρ leads to inverse relationship:

$$\hat{\rho}(\mathbf{t}) = \hat{g}(\mathbf{t}) \tau \eta^{-1} e^{\tau z_1}, \quad (17)$$

which shows immediately that the problem is exponentially ill-posed, and any arbitrary small high frequency noise present in the measurements grows without bound being multiplied by the exponential term $e^{\tau z_1}$. Therefore, to avoid unstable reconstruction algorithms, we introduce regularizing constraints. For the problem with the functional J_0 , optimality conditions lead to the regularized solution with the Fourier transform $\hat{\rho}_0(\mathbf{t})$:

$$\hat{\rho}_0(\mathbf{t}) = \left[\frac{e^{-\tau z_1} \eta}{e^{-2\tau z_1} \eta^2 + \alpha \tau} \right] \hat{g}(\mathbf{t}). \quad (18)$$

For the problem with the functional J_1 , Fourier transform of the regularized solution $\hat{\rho}_1(\mathbf{t})$ satisfies

$$\hat{\rho}_1(\mathbf{t}) = \left[\frac{e^{-\tau z_1} \eta}{e^{-2\tau z_1} \eta^2 + \alpha \tau^3} \right] \hat{g}(\mathbf{t}). \quad (19)$$

Eq. (19) is a Fourier transform of eq. (B9) resolved for the function ρ . Eq. (18) is obtained similarly from the analogous (B9) equation for the functional J_0 . The terms $\alpha \tau$ and $\alpha \tau^3$ in the denominator show the regularizing effect of the added stabilization functionals: for large values of τ the impact of the first term is negligibly small. The comparative value of the two terms in the denominator shows how much the solution is perturbed due to the regularized scheme.

The quadratic functionals discussed are easy to implement, they lead to computationally efficient numerical schemes. However, due to the presence of the terms $\alpha \tau$ and $\alpha \tau^3$ in (18) and (19), these numerical schemes impose restrictions on the ‘sharpness’ of the solution.

5 NON-SMOOTH REGULARIZATION

An alternative to smooth regularization is to use a functional that does not penalize sharp changes in properties (discontinuities). A number of such functionals has been recently introduced in inversion schemes dealing with image processing. These functionals usually have a form

$$J(\rho) = \int \phi(\rho), \quad (20)$$

where the function $\phi(\rho)$ is chosen to be a non-quadratic, as in Geman & Yang (1995),

$$\phi(\rho) = \frac{|\nabla \rho|^2}{1 + |\nabla \rho|^2}, \quad (21)$$

or as in Morel & Solimini (1995):

$$\phi(\rho) = |\nabla \rho|^p, \quad p > 1. \quad (22)$$

Smoothing functionals J_0 and J_1 are also particular cases of eq. (20), however, with a quadratic function $\phi(\rho)$. When $\phi(\rho) = \rho^2$, we obtain the functional J_0 . If $p = 2$ in (22), this leads to the functional J_1 .

To prevent penalization of sharp changes of the density function in the minimization problem, we use the variation of the solution ρ in the domain Ω as the stabilizing functional:

$$\min_{\rho} P_{TV}^{\alpha}(\rho, g) = \min_{\rho} (\|K\rho - g\|_2^2 + \alpha J_{TV}(\rho)). \quad (23)$$

The variation of a function (Giusti 1984) is a total change of the values of the function in the domain. It sums up the jumps of the function at discontinuity points and its variation in the intervals where the function is continuous. When the function ρ is differentiable, $J_{TV}(\rho)$ is:

$$J_{TV}(\rho) = \int_{\Omega} |\nabla \rho| d\mathbf{r}. \quad (24)$$

We will use this expression understanding that if the function is discontinuous at some point, its variation there is just the size of the jump. For example, if a function is zero on the interval from zero to 0.5, and then it jumps and is equal to one on the rest of the interval, its variation is one.

The functional $J_{TV}(\rho)$ is a particular kind of eq. (20) when $\phi(\rho) = |\nabla \rho|$. It was considered among other functionals in a number of works in image reconstruction. It is shown in Vogel (1997) that the minimization problem (23) is well posed, when the operator K is a first kind integral operator (in 2-D) with a continuous kernel.

The gravimetric integral operator (3) (in 2-D) is a particular kind of such operator. Similar arguments can be used to show that the minimization problem when K is a first kind integral operator in 3-D is well posed (Vogel 1998).

To solve (23), we derive the Euler–Lagrange equation and use the gradient of the parametric functional in an adaptive gradient minimization scheme. For the first term in (23), the Euler–Lagrange equation is,

$$(K^*K\rho - K^*g) = 0. \quad (25)$$

For minimization of the total variation stabilization functional in (23), the gradient of J_{TV} is derived in Appendix C. The resulting Euler–Lagrange equation is

$$(K^*K\rho - K^*g) + \alpha \nabla \cdot \frac{\nabla \rho}{\sqrt{|\nabla \rho|^2 + \beta}} = 0. \quad (26)$$

Because the minimization problem (23) is non-quadratic, the obtained problem (26) and a corresponding problem for a smoothing stabilizer J_0 or J_1 are essentially different. The problem (12) is a linear problem and its discretization leads to a well posed finite dimensional problem. In (26) we encounter a problem of solving integro-differential equation, and the previous technique does not apply. Moreover, the problem (26) is non-linear, and to develop a solution technique, we first need to linearize it. Having rewritten eq. (26) as

$$\nabla \cdot \sigma \nabla \rho = \frac{1}{\alpha} (K^*g - K^*K\rho), \quad (27)$$

where we denote the term $(\sqrt{|\nabla \rho|^2 + \beta})^{-1}$ as σ , we can observe that (27) is the equation of ‘conductivity type’. Data misfit plays a role of a current source term, while the ‘properties’ σ depend on the solution. This suggests a possible iterative way of solution of (27) which is similar to a method used in image reconstruction works (Rudin *et al.* 1992; Chan *et al.* 1996; Vogel & Oman 1996). Fix $\rho(\mathbf{r})$, calculate data misfit and the ‘conductivity’ σ , solve the electric conductivity problem with data misfit taken as a source. The solution gives an updated distribution of the density $\rho(\mathbf{r})$. Take this solution as a new fixed $\rho(\mathbf{r})$, again calculate data misfit and the ‘conductivity’ σ , and so on.

The known properties of the solution of a conductivity problem suggest also an interpretation of TV regularization and explain its non-smoothing behaviour. The solution of a conductivity problem is known to change rapidly and to have larger gradients in regions of low conductivity versus an almost constant solution with zero gradient in the high conductivity regions. For problem (27), this means that the density function ρ changes more rapidly and has larger gradients in the regions where the value of σ calculated from the previous iteration is small. On the contrary, the function ρ is constant in the regions where σ is very big. However, σ is the reciprocal value of the gradient of the solution calculated on the previous iteration, and it is small in the regions where the gradient of the density ρ is large. Hence, during the course of iterations, the density function ρ is not smoothed but becomes more and more contract to be driven to a sharp contrast solution. This analysis shows that the total variation stabilization can be efficient in recovering non-smooth geophysical properties.

6 NUMERICAL IMPLEMENTATION

Different approaches in Rudin *et al.* (1992), Chan *et al.* (1996), Vogel & Oman (1996) and Bertete-Aguirre (1997) have been used

to minimize problem (23). In this work, we discretize the forward operator K and the gradient of the TV functional, and then use a steepest descent minimization to find the solution of the regularized finite-dimensional problem. The solution ρ is constructed as a minimizer of the functional (23) using an iterative gradient minimization scheme. We start with some large value of the regularization parameter α . On each iteration step k , we calculate the descent direction Γ_k given by negative gradient of the parametric functional (23) at the point $\rho^{(k)}$,

$$\Gamma_k = - \left. \frac{\partial P_{TV}^\alpha(\rho, g)}{\partial \rho} \right|_{\rho=\rho^{(k)}}. \quad (28)$$

Calculation of the former (see Appendix C) results in:

$$\Gamma_k = - (K^*K\rho^{(k)} - K^*g) - \alpha \nabla \cdot \frac{\nabla \rho^{(k)}}{\sqrt{|\nabla \rho^{(k)}|^2 + \beta}}. \quad (29)$$

Using the line search we calculate the length of the step τ in the direction of the steepest descent which minimizes the value of the parametric functional,

$$P_{TV}^\alpha(\rho^k + \tau \Gamma_k, g) \rightarrow \min_\tau. \quad (30)$$

Having calculated the value τ of the step in the descent direction, we update the solution

$$\rho^{(k+1)} = \rho^{(k)} + \tau \Gamma_k. \quad (31)$$

The calculated density $\rho^{(k+1)}$ is used for evaluating the gradient (29) of the functional on the next iteration step. Starting with a large value of α , the changes in the values of the functional are monitored, and α is decreased every time when the difference in residuals is less than a predetermined threshold.

To introduce discretization, we consider 2-D problem assuming that the density is constant in y -direction, and represent a rectangular domain Ω of the size $l_x \times l_z$, as a union of small rectangular blocks: $\Omega = \{\Omega_{ij}, i = 1, \dots, nx, j = 1, \dots, nz\}$. The function $\rho(\mathbf{r})$, $\mathbf{r} = (x, z)$, is a piecewise constant function:

$$\rho(\mathbf{r}) = \sum_{i=1}^{nx} \sum_{j=1}^{nz} \rho_{ij} \chi_{ij}(\mathbf{r}), \quad \mathbf{r} \in \Omega, \quad (32)$$

where

$$\chi_{ij}(\mathbf{r}) = \begin{cases} 1, & \mathbf{r} \in \Omega_{ij} \\ 0, & \text{otherwise.} \end{cases} \quad (33)$$

Substituting this in the forward operator (3), we obtain a finite dimensional approximation:

$$g(\mathbf{r}') = \sum_{i=1}^{nx} \sum_{j=1}^{nz} \rho_{ij} \int_{\Omega_{ij}} \mathcal{K}(\mathbf{r}', \mathbf{r}) d\mathbf{r} \quad (34)$$

with ρ_{ij} being constant. We use an analytic solution of the 2-D forward gravity problem for a rectangular prism (Telford *et al.* 1990) to evaluate integrals in (34). Restoring dropped universal gravitational constant γ , we have

$$g_{ij} = 2\gamma a \rho_{ij}. \quad (35)$$

Here

$$a = D\theta_2 - d\theta_1 - x \log\left(\frac{r_1 r_4}{r_2 r_3}\right) + b \log\left(\frac{r_4}{r_3}\right), \quad (36)$$

and all the parameters refer to the i, j -th cell of discretization. Fig. 1 shows the parameters in (35)–(36).

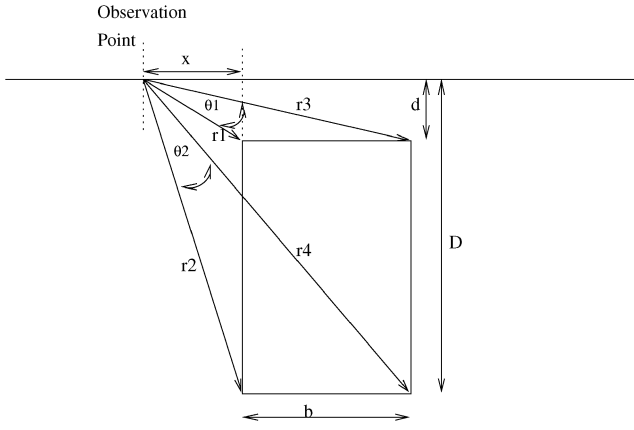


Figure 1. Geometrical parameters of a prism introduced for calculation of a generated gravitational potential.

Having discretized the subsurface region, we introduce a cell centred finite difference approximation for the gradient of the objective functional. We use the same notation for the vectors obtained from discretization of the functions ρ and g , and for the matrix K . Discretization of the gradient of the data misfit is straightforward. To show discretization of the gradient of the TV functional we introduce $h_x = l_x/n_x$ and $h_z = l_z/n_z$ and a discrete gradient with the entries $\nabla_{i,j}$:

$$\nabla_{i,j}\rho = \left(\frac{\rho_{i+1,j} - \rho_{i,j}}{h_x}, \frac{\rho_{i,j+1} - \rho_{i,j}}{h_z} \right). \quad (37)$$

Discretized gradient of the TV functional can be written as a 2-D vector with the elements of the form:

$$\nabla_{i,j}^T \frac{\nabla_{i,j}\rho}{\sqrt{|\nabla_{i,j}\rho|^2 + \beta}}. \quad (38)$$

Let $q_{i,j}$ be the term with the square root in the denominator:

$$q_{i,j} = \frac{1}{\sqrt{|\nabla_{i,j}\rho|^2 + \beta}}. \quad (39)$$

Then, exploiting eq. (37) results in $q_{i,j}$ having the value

$$\left(\left(\frac{\rho_{i+1,j} - \rho_{i,j}}{h_x} \right)^2 + \left(\frac{\rho_{i,j+1} - \rho_{i,j}}{h_z} \right)^2 + \beta \right)^{-\frac{1}{2}}. \quad (40)$$

Now, if we use (37) in (38), the i, j -th element of the discretized gradient can be readily calculated as:

$$\frac{Q_x^{ij}}{h_x^2} + \frac{Q_z^{ij}}{h_z^2} \quad (41)$$

with

$$Q_x^{ij} = \rho_{i+2,j} q_{i+1,j} + \rho_{i,j} q_{i,j} - \rho_{i+1,j} (q_{i+1,j} + q_{i,j}),$$

$$Q_z^{ij} = \rho_{i,j+2} q_{i,j+1} + \rho_{i,j} q_{i,j} - \rho_{i,j+1} (q_{i,j+1} + q_{i,j}).$$

7 RESULTS OF NUMERICAL SIMULATIONS

For numerical simulations we used several models with a piecewise density function that exhibits sharp density contrast and sharp edges. The first model is a model of a fault shown in Fig. 2. The observations

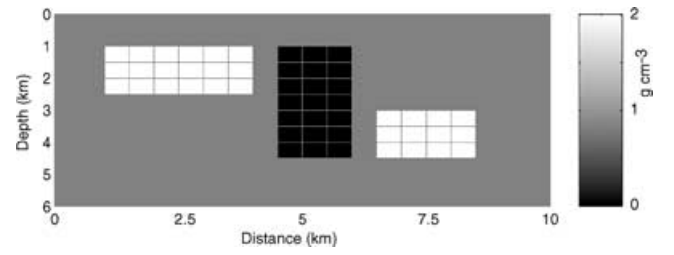


Figure 2. Distribution of the density for the fault model.

are performed on the earth surface in 267 stations aligned in the horizontal direction x .

We consider initially only computer noise added during the computing of the numerical solution, then we added 6 per cent Gaussian noise to the measured data to numerically study stability and robustness of the algorithm in the presence of noise in observations. The regularization parameter was allowed to decrease until no improvement in the solution was obtained due to the presence of low level amplitude noise.

Fig. 3 shows an attempt to recover the density function when the norm of the 2-D gradient of the solution is used as a stabilization functional. The domain is divided in 240 cells, which turns the problem into highly ill-posed one. The solution is obtained using an adaptive gradient minimization. The starting model was the true model shown in Fig. 2 with added 25 per cent random noise. Starting with the ‘true’ model emphasizes the effect that the regularization term has on the final model. The result of inversion is shown in Fig. 3. The inverted density function has the correct range of values, but it is very smooth. The inversion procedure fails to recover the non-smooth density distribution in spite of information contained in the starting model. The structural information contained in the starting model was ‘smoothed’ out in the minimization procedure due to the 2-D gradient penalty term.

Inversion results with the TV stabilization functional are shown in Figs 4 and 5. The starting model and discretization used in this simulation were the same as in the previous example. Fig. 4 shows the reconstructed density function after 19 iterations as an intermediate result of inversion. Fig. 5 shows results of inversion of noisy data: 6 per cent Gaussian noise was added to the gravitational observations. The reconstructed density, though not perfectly blocky, is

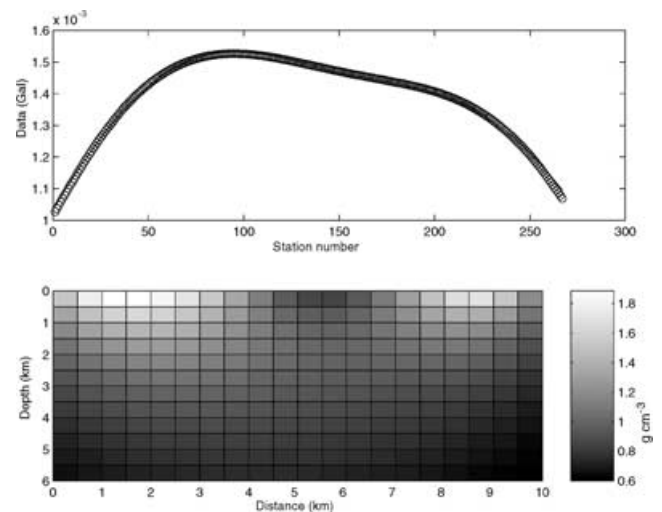


Figure 3. Solution for the fault model using a smoothing regularization scheme together with the observed and predicted data on the top.

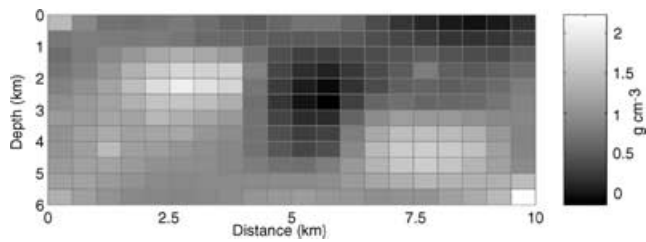


Figure 4. TV regularization: Intermediate solution for the fault model constructed using the 2-D total variation regularization scheme (density function after 19 iterations).

closer to the non-smooth function. Hence the method based on TV stabilization is able to recover a contrast density function preserving information available in the starting model without ‘smoothing’ it in the stabilized inversion procedure.

As it was mentioned before, there are many practically important situations where non-smooth density distributions give a better picture of the earth model. Initial models presenting these features are often available from previous research in the area, but as it was shown, smoothing inversion techniques would not preserve this information. Results presented here show that the quadratic penalty term smoothes the solution destroying the information about the model sharpness even if we start from the true solution or a density function that is very close to the true solution. On the other hand, TV stabilization functional does not have this smoothing feature and drives the iterative model to a more contrast density distribution.

Another model used in simulations was the dipped fault model. The true distribution of the density is shown in Fig. 6. We discretize the 2-D density function and obtain the model consisting of 240 cells. The density function is assumed to be constant in each cell. This discrete model roughly represents a dipped geological fault.

In this numerical example, measurements of the vertical component of the gravity field are simulated assuming they are taken on the surface of the Earth. The measured vertical anomaly is shown in the top plot in Fig. 6. Fig. 7 shows a model of the density that we use as initial model for the density distribution starting the inversion procedure. The initial model for this simulation was the true model of the fault (Fig. 6) with added 25 per cent noise. Graphs on the top in Fig. 7 show the vertical gravity field generated by this model together with the measured data corresponding to the true model. The solid line corresponds to measured data, circles ‘o’ are used to show data due to the initial model. This difference between the measured data and the values calculated from the model density distribution is used to form the misfit functional and then to compute the gradient of the misfit functional augmented with the TV stabilization functional. Figs 8 and 9 show the evolution of the misfit functional and of the stabilization functional during the iteration scheme. In first iteration steps, the data misfit functional has

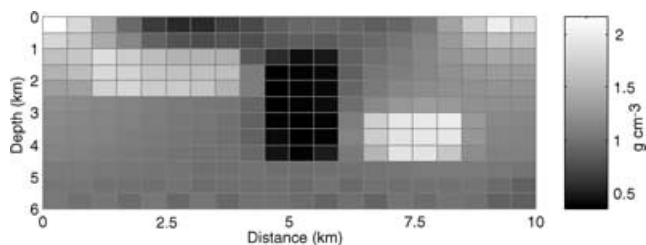


Figure 5. TV regularization: Solution for the fault model with noisy data using the 2-D total variation regularization scheme.

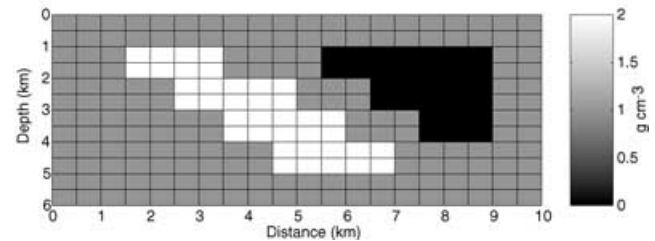
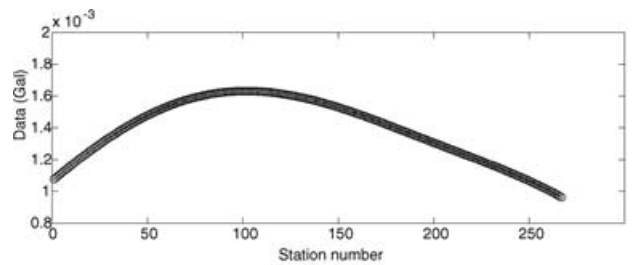


Figure 6. Bottom figure shows distribution of the density modelling a dipped fault. Top figure shows vertical gravity field generated on the surface at 267 observation points.

almost constant value. The stabilization functional, however, fast decreases in the beginning of iterative process. Practically, due to large values of the regularization parameter in the beginning of iterations, only the stabilization functional is subject to minimization. Later, the data misfit functional starts to play more important role, and the value of the stabilization functional stays almost constant. The misfit functional fast decreases in the middle, however, later the convergence slows down. This corresponds to the well-known effect of slow convergence in the domain close to the minimum value of the functional.

The inversion results using TV regularization method are shown in Fig. 10, which demonstrates the reconstructed density function after 179 iterations. We can see that the TV method still is able to recover part of the non-smooth features of the true model.

The last numerically simulated model was a model of a salt dome oil reservoir. Bottom figure in Fig. 11 shows geometry of a salt dome oil reservoir. For this simulation, measurements are assumed to be

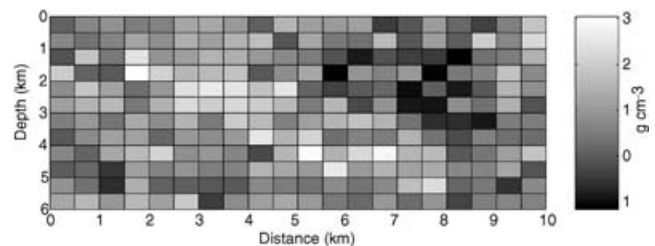
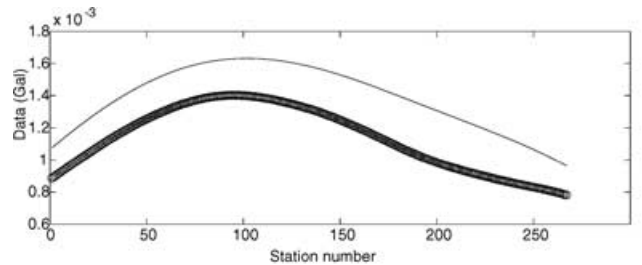


Figure 7. Starting model of the density distribution for the dipped fault model. Top figure shows vertical gravity field generated by this model. Solid line corresponds to measured data, ‘o’ show data due to the initial model.

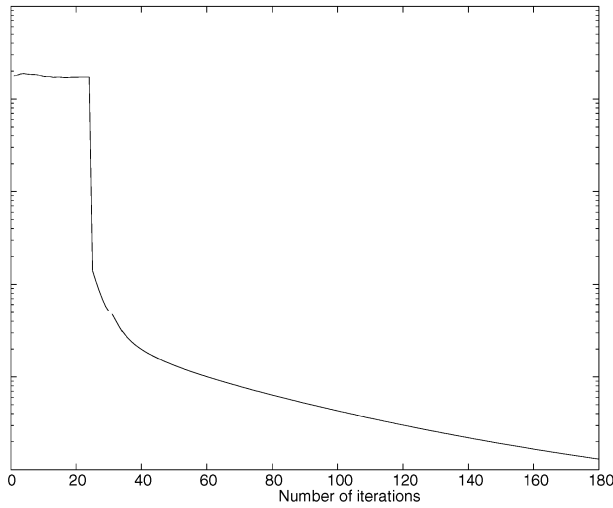


Figure 8. Changing of the misfit functional in the course of the iteration procedure (solution for the dipped fault model).

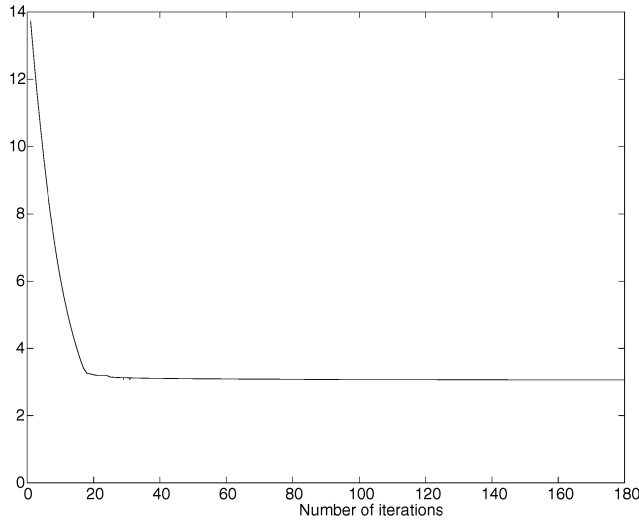


Figure 9. The values of the total variation stabilization functional (solution for the dipped fault model).

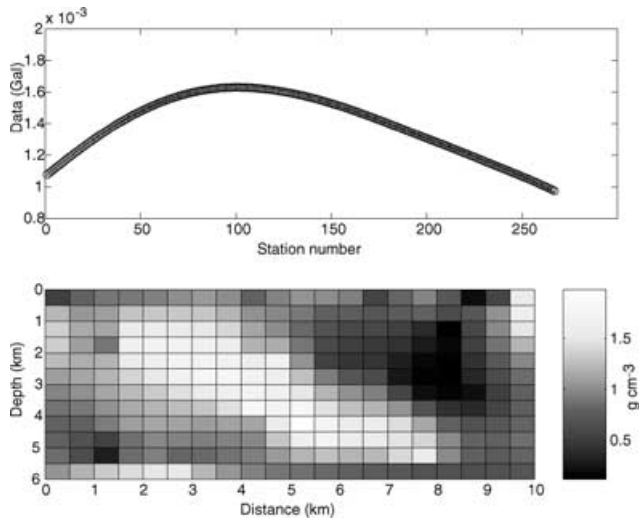


Figure 10. TV regularization: Reconstructed density for the dipped fault model using the total variation penalization scheme.

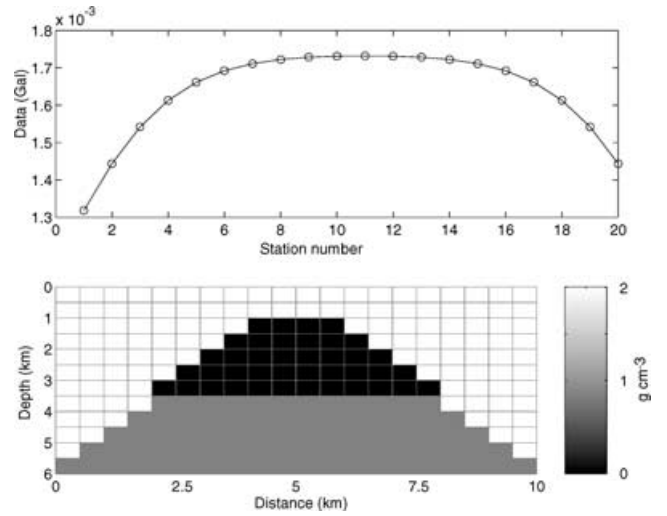


Figure 11. Bottom figure shows a model of the distribution of the density for oil reservoir simulation. Top figure shows vertical gravity field generated by this model.

taken in a horizontal borehole below the reservoir. We assume that the measurements are contaminated with 5 per cent noise. We show a density function for the oil reservoir in Fig. 11, the model being discretized in 240 cells. The starting model for the oil reservoir simulation was the true model with added 25 per cent noise. The destructive influence of this amount of noise on the true model can be appraised from comparison of the models for dipped fault simulation depicted in Fig. 6 for the true model and Fig. 7 with added 25 per cent noise. The solution of the inverse gravimetric problem for the salt dome oil reservoir model with the TV regularization scheme is shown in Fig. 12. The display in Figs 11 and 12 shows depth in vertical direction so that the zeroth layer of the blocks corresponds to the surface structures. The measurements now take place at the horizontal borehole at the bottom of the model.

The presence of 5 per cent noise in the gravity data limits the accuracy in the inversion scheme, which is reflected in the quality of the recovered density distribution. However, the inversion results

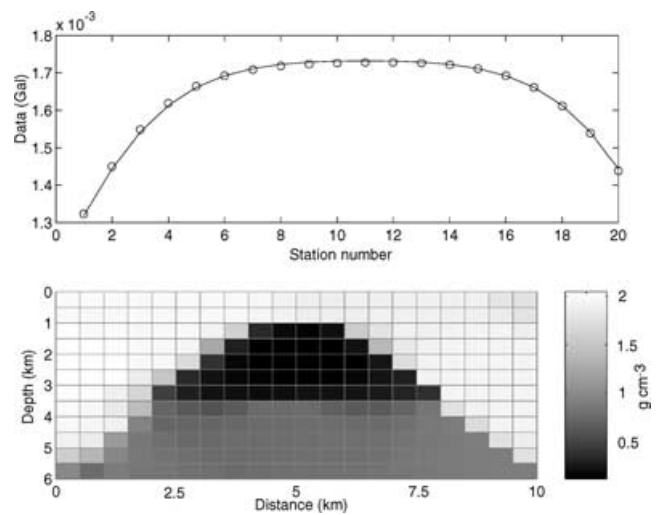


Figure 12. Bottom figure gives the reconstructed density function for the oil reservoir model. Reconstruction using the TV regularization scheme. Top figure shows generated vertical gravity field. Solid line corresponds to measured data, 'o' show data due to the calculated density model.

show that the TV method still is able to recover part of the non-smooth features of the true models. In spite of the presence of noise in the gravity data, the constructed solution is close to the true density distribution. This illustrates numerically the stability of the TV reconstruction algorithm.

8 CONCLUSION

Stabilization of inversion methods with smoothing functionals can result in oversmoothed reconstructions of Earth's interior properties. We suggest the use of the total variation of the model parameters as a stabilization functional to preserve sharp features in inverted models. Examples show that this approach can recover sharp contrast density functions. The adaptive gradient minimization shows to be an efficient scheme for this problem. The approach is especially effective in situations when prior information about the geological structure is available.

ACKNOWLEDGMENTS

We would like to thank Curtis R. Vogel for helpful discussions of the problem. We also would like to thank Kabir Roy-Chowdhury, Pavel Ditmar and another reviewer of the paper for constructive comments. This work was supported by Schlumberger-Doll Research. E. Cherkhev was partially supported by DOE OBES under grant number DE-FG03-93ER14313.

REFERENCES

- Backus, G.E., 1968. Application of a non-linear boundary-value problem for Laplace's equation to gravity and geomagnetic intensity surveys, *Quart. J. Mech. Appl. Math.*, **21**, 195–221.
- Backus, G.E., 1970. Non-uniqueness of the external geomagnetic field determined by surface intensity measurements, *J. geophys. Res.*, **75**, 6339–6341.
- Bassrei, A., 1993. Regularization and inversion of 2D Gravity Data, *63th. SEG Ann. Mtg., Expanded Abstracts* 405–409.
- Bertete-Aguirre, H., 1997. Reconstruction of non-smooth solutions of ill-posed geophysical inverse problems, *PhD thesis, COPPE, Federal University of Rio de Janeiro*.
- Bertete-Aguirre, H. & Xavier, A., 1994. Mínimos cuadrados aplicados à inversão geofísica, *Coppe-Sistemas Report*, Federal University of Rio de Janeiro.
- Bhattacharyya, B.K., 1967. Some general properties of potential fields in space and frequency domain: A review, *Geoexploration*, **5**, 127–143.
- Chan, T.F., Golub, G.H. & Mulet, P., 1996. A nonlinear primal-dual method for total variation-based image restoration, *ICAOS'96, Paris*, 241–252.
- Cherkheva, E., 1990. Estimation of unremovable uncertainty in the determination of the components of the geomagnetic field, *Izv. Akad. Nauk SSSR Ser. Fiz. Zemli (Physics of Solid Earth)*, **4**, 289–294.
- Constable, S.C., Parker, R.L. & Constable, C.G., 1987. Occam's inversion: A practical algorithm for generating smooth models from electromagnetic sounding data, *Geophysics*, **52**, 289–300.
- Dobson, D. & Santosa, F., 1994. An image-enhancement technique for electrical impedance, *Inverse Problems*, **10**, 317–334.
- Erdelyi, A., Magnus, W., Oberhettinger, F. & Tricomi, F.G., 1954. Tables of Integral Transforms, McGraw-Hill, New York.
- Geman, D. & Yang, C., 1995. Nonlinear image recovery with half-quadratic regularization, *IEEE Trans. Image Proc.*, **4**, 932–945.
- Giusti, E., 1984. Minimal Surfaces and Functions of Bounded Variation, Birkhauser, Boston.
- Green, W.R., 1975. Inversion of gravity profiles by use of a Backus-Gilbert approach, *Geophysics*, **40**, 763–772.

- Guillen, A. & Menichetti, V., 1984. Gravity and magnetic inversion with minimization of a specific functional, *Geophysics*, **49**, 1354–1360.
- Hansen, P.C. & O'Leary, D.P., 1993. The use of the L-curve in the regularization of discrete ill-posed problems, *SIAM J. Sci. Comput.*, **14**, 1487–503.
- Isakov, V., 1990. Inverse source problems: Mathematical Surveys and Monographs, **34**, AMS, Providence.
- Kolesova, V. & Cherkheva, E., 1987. A vector model of the magnetic field based on a system of dipole sources, *Geomagnetism and Aeronomy*, **27**, 151–153.
- Last, B.J. & Kubik, K., 1983. Compact gravity inversion, *Geophysics*, **48**, 713–721.
- Lavrentiev, M.M., Romanov, V.G. & Shishatsky, S.P., 1980. Ill-posed problems in mathematical physics and analysis, Nauka, Moscow.
- Li, Y. & Oldenburg, D.W., 1998. 3-D inversion of gravity data, *Geophysics*, **63**, 109–119.
- Morel, J.-M. & Solimini, S., 1995. Variational methods in image segmentation, Burkhauser, Boston.
- Novikov, P.S., 1938. Sur le probleme inverse du potentiel, *Comptes Rendus de l'Academie des Sciences de l'URSS (Doklady Akad. Nauk SSSR)*, **18**, 165–168.
- Parker, R.L., 1973. The rapid calculation of potential anomalies, *Geophys. J. R. astr. Soc.*, **31**, 447–455.
- Portniaguine, O. & Zhdanov, M.S., 1999. Focusing geophysical inversion images, *Geophysics*, **64**, 874–887.
- Rudin, L.I., Osher, S. & Fatemi, E., 1992. Nonlinear total variation based noise removal algorithms, *Physica D*, **60**, 259–268.
- Sabatier, P.C., 1977. Positivity constraints in linear inverse problems—I. General theory—II. Applications, *Geophys. J. R. astr. Soc.*, **48**, 415–441, 443–459.
- Strakhov, V.N. & Brodsky, M.A., 1986. On the uniqueness of the solution of the inverse logarithmic potential problem, *SIAM J. Appl. Math.*, **46**, 324–344.
- Strakhov, V.N. & Valyashko, G.M., 1984. Adaptive regularization of linear ill-posed problems and their use in the solution of problems of gravimetry and magnetometry, *Izv. Akad. Nauk SSSR Ser. Fiz. Zemli (Physics of Solid Earth)*, **11**, 55–77.
- Telford, W.M., Geldart, L.P. & Sheriff, R.E., 1990. Applied Geophysics, Cambridge University Press, Cambridge.
- Tikhonov, A.N. & Arsenin, V.Y., 1977. Solutions of ill-posed problems, Wiley, New York.
- Vogel, C.R., 1997. Nonsmooth regularization, in *Inverse Problems in Geophysical Applications*, pp. 1–11, eds Engl, H.W., Louis, A. & Rundell, W., SIAM, Philadelphia.
- Vogel, C.R., 1998. Private communication.
- Vogel, C.R. & Oman, M.E., 1996. Iterative methods for total variation denoising, *SIAM J. Sci. Comput.*, **17**, 227–238.

APPENDIX A: NON-UNIQUENESS OF THE INVERSE PROBLEM FOR NEWTONIAN POTENTIAL

Consider a twice differentiable function u_1 , that is zero together with its derivatives outside some region Ω_1 inside the domain Ω . Let a function ρ_1 equal a laplacian of u_1 scaled by a coefficient (-4π). Because the function u_1 and its derivatives are zero outside Ω_1 , the density function ρ_1 is different from zero also only in the region Ω_1 ,

$$\Delta u_1 = -4\pi\rho_1, \quad \mathbf{r} \in \Omega_1. \quad (\text{A1})$$

Now, if a true density distribution is a sum $\rho + \rho_1$, then Poisson's equation becomes

$$\Delta(u + u_1) = -4\pi(\rho + \rho_1), \quad \mathbf{r} \in \Omega. \quad (\text{A2})$$

Measuring the vertical component of the gradient outside Ω_1 we register only function $\partial u/\partial z'$, but not the function $\partial u_1/\partial z'$. Hence these data give information only about the density function ρ , but not

the function ρ_1 . This shows that measuring potential fields (or components of their gradients) on the boundary of the region containing anomalous density, we cannot distinguish a true density function in a class of functions satisfying described requirements.

APPENDIX B: THE EULER EQUATION FOR QUADRATIC STABILIZATION PROBLEM

The Euler-Lagrange equation for solution of the optimization problem (8) with the quadratic functional J_1 , is derived varying the functional $P^\alpha(\rho, g)$ with respect to ρ . Variation of the functional $P(\rho, g)$ leads to the following expression:

$$\begin{aligned} \delta P(\rho, g) &= \int_{\Omega} \delta\rho(\mathbf{r}) \int_{\partial\Omega} \mathcal{K}(\mathbf{r}', \mathbf{r}) \\ &\quad \times \left(\int_{\Omega} \rho(\mathbf{r}'') \mathcal{K}(\mathbf{r}', \mathbf{r}'') d\mathbf{r}'' - g(\mathbf{r}') \right) d\mathbf{r}' d\mathbf{r}. \end{aligned} \quad (\text{B3})$$

Variation of the stabilization functional

$$\delta \int_{\Omega} |\nabla\rho(\mathbf{r})|^2 d\mathbf{r}, \quad (\text{B4})$$

gives an additional term,

$$\int_{\partial\Omega} \delta\rho(\mathbf{r}') \frac{\partial\rho}{\partial n} d\mathbf{r}' - \int_{\Omega} \delta\rho(\mathbf{r}) \Delta\rho(\mathbf{r}) d\mathbf{r}, \quad (\text{B5})$$

where Δ is laplacian. The Euler equations are obtained by setting the coefficients of $\delta\rho$ to zero. This permitted us to drop 2 in (B3) and (B5). On the boundary $\partial\Omega$ we have,

$$\frac{\partial\rho(\mathbf{r}')}{\partial n} = 0, \quad \mathbf{r}' \in \partial\Omega. \quad (\text{B6})$$

We assume that the eq. (B6) is always satisfied as we deal with an isolated anomaly model. In the region Ω , we have two terms: The first term E_M , comes from varying the misfit functional, E_M equals to

$$\int_{\partial\Omega} \mathcal{K}(\mathbf{r}', \mathbf{r}) \left(\int_{\Omega} \rho(\mathbf{r}'') \mathcal{K}(\mathbf{r}', \mathbf{r}'') d\mathbf{r}'' - g(\mathbf{r}') \right) d\mathbf{r}'. \quad (\text{B7})$$

The second term arrives from varying the stabilization functional multiplied by α :

$$E_S = -\alpha \Delta\rho(\mathbf{r}). \quad (\text{B8})$$

The optimality condition requires the sum of these two terms to be zero: $E_M + E_S = 0$. Hence, the Euler equation can be written as

$$\begin{aligned} \int_{\partial\Omega} \mathcal{K}(\mathbf{r}', \mathbf{r}) \int_{\Omega} \rho(\mathbf{r}'') \mathcal{K}(\mathbf{r}', \mathbf{r}'') d\mathbf{r}'' d\mathbf{r}' - \alpha \Delta\rho(\mathbf{r}) \\ = \int_{\partial\Omega} \mathcal{K}(\mathbf{r}', \mathbf{r}) g(\mathbf{r}') d\mathbf{r}'. \end{aligned} \quad (\text{B9})$$

APPENDIX C: GRADIENT OF THE TOTAL VARIATION FUNCTIONAL

The gradient of the total variation functional can be derived by the following way:

$$\delta_\rho \int_{\Omega} |\nabla\rho| d\mathbf{r} = \int_{\Omega} \frac{\nabla\rho \cdot \nabla\delta\rho}{|\nabla\rho|} d\mathbf{r}. \quad (\text{C10})$$

Integrating by parts recasts the previous integral as

$$\int_{\partial\Omega} \frac{\delta\rho}{|\nabla\rho|} \frac{\partial\rho}{\partial n} ds - \int_{\Omega} \delta\rho \left(\nabla \cdot \frac{\nabla\rho}{|\nabla\rho|} \right) d\mathbf{r}. \quad (\text{C11})$$

The optimality condition is satisfied if

$$\nabla \cdot \frac{\nabla\rho}{|\nabla\rho|} = 0 \quad \text{in } \Omega, \quad \frac{\partial\rho}{\partial n} = 0 \quad \text{on } \partial\Omega. \quad (\text{C12})$$

The second of these equations is satisfied if we deal with an isolated mass anomaly, which is a standard assumption for geophysical inverse problems. The lefthand side of the first equation gives us the gradient of the TV functional.

Due to the term $1/|\nabla\rho|$ in the eq. (C12), the functional J_{TV} is non-differentiable when $|\nabla\rho| = 0$. To avoid singularity, we introduce a small positive parameter β , and approximate $|\nabla\rho|$ as:

$$|\nabla\rho| \cong \sqrt{|\nabla\rho|^2 + \beta}. \quad (\text{C13})$$

This corresponds to approximation of the non-differentiable functional J_{TV} by a differentiable one:

$$\int_{\Omega} |\nabla\rho| d\mathbf{r} \cong \int_{\Omega} \sqrt{|\nabla\rho|^2 + \beta} d\mathbf{r}. \quad (\text{C14})$$

Such an approximation is continuous (Vogel & Oman 1996). The resulting gradient of the total variation functional is

$$\frac{\partial J_{TV}}{\partial\rho} = \nabla \cdot \frac{\nabla\rho}{\sqrt{|\nabla\rho|^2 + \beta}}. \quad (\text{C15})$$